Temperature Polarization in Mass Transport Through Hydrophobic Porous Membranes

L. Martínez-Díez and M. I. Vázquez-Gonzàlez
Dept. de Física Aplicada, Universidad de Málaga, 29071-Málaga, Spain

Membrane distillation is a membrane process in which two liquid phases at different temperatures are separated by a microporous hydrophobic membrane. The membrane plays the role of physical support for the vapor-liquid interface. Pure water transport through PTFE and PVDF flat membranes was studied, as well as the dependence of the phenomena on average temperature and recirculation rate at membrane sides. The influence of these operating conditions on mass transfer is also discussed, taking into account mass and heat transfer within the membrane and adjoining liquid phases. The concept of temperature polarization introduced into the transport equations shows its importance in experimental results.

Introduction

Membrane distillation is a temperature-driven process in which two liquids or solutions at different temperatures are separated by a microporous membrane. The liquids or solutions must not wet the membrane, so that only vapor (and not liquid) is present in the pores. In this way the imposed transmembrane temperature gradient induces a vapor-pressure gradient across the hydrophobic microporous membrane. Vapor molecules will migrate through the membrane from the high-vapor-pressure side where they evaporate to the low-vapor-pressure side where they condense. To avoid getting wet, the maximum pore size must be small (< 1 μm), and the surface tension of the liquid high. Hydrophobic microporous membranes such as those made from polypropylene (PP), polytetrafluoroethylene (PTFE), and polyvinylidenefluoride (PVDF) meet these requirements.

The membrane distillation process has been studied much in the last ten years, and its potential application in desalination (Drioli and Wu, 1985; Anderson et al., 1985; Ohta et al., 1990; Enoch et al., 1994), juice concentration (Sheng et al., 1991), separation of alcohol-water mixtures (Nakao et al., 1987; Hoffmann et al., 1987), wastewater treatment (Calabro et al., 1991) as well as in other applications (Calabro et al., 1990) has been proven.

The main advantages of using membrane distillation when compared with conventional distillation processes are: lower operating temperatures, mist elimination, and the possibility of overcoming corrosion problems by using plastic equipment (Gostoli and Sarti, 1989). The attractiveness of this process comes from the fact that it can use available energy sources such as solar energy or waste energy in industrial processes. However, this process is still suffering from high membrane costs and the danger of membrane wetting, as reported by Banat and Simandl (1994).

Heat transfer plays an important role in the mass transfer through these membranes: the vapor flux varies with the temperature difference between the membrane walls, and this difference depends to a large extent on the heat-transfer characteristics of the membrane module. In fact, the need to supply heat to the evaporation surface of the membrane means that the temperature gradients must be in the liquid phase adjacent to the membrane. The same occurs in the condensation surface side. In this way, the effective temperature difference between the two sides of the membrane is lower than the temperature difference between the bulk solutions.

This loss of driving force brought about by thermal gradients in the fluids bounding the membrane is known as temperature polarization. This concept was introduced by Vink and Chisthi (1976) after studying another transport phenomenon (thermal osmosis) through membranes, which is also based on the existence of a temperature gradient between the two sides. The importance of this polarization phenomenon in thermal osmosis has been analyzed by Bellucci (1981), but is frequently left aside when analyzing the distillation process using membranes.

In the present work we have studied the water distillation process using three different membranes for different operating conditions. Mass- and heat-transfer theories have been

applied to membrane and adjoining fluids in order to show the importance of the temperature polarization.

Experimental

Membrane characterization

One PVDF and two PTFE membranes have been studied. The PTFE membranes are marketed by Gelman Instruments Co. as TF-200 and TF-450 with a nominal pore size of 0.2 and 0.45 μm and a porosity of 0.80. These membranes have a limited mechanical strength, and in practice they must be supported by different nets. In this way, they are composite membranes formed by an actual porous PTFE layer with a thickness of 60 μm on a polypropylene screen support which has a pore diameter greater than 500 μm. The PVDF membrane is marketed by Millipore as Durapore HVHP, with a 0.45-μm nominal pore size, 0.70 porosity, and 125-μm thickness.

The liquid employed in the experiments was pure doubly distilled deionized water.

To obtain a better knowledge of the membrane structure, scanning electron micrographs of the surfaces of the membranes have been carried out and all the membranes exhibit pores of various sizes. To quantify these pore sizes, measurements of Hg porometry and measurements of gas-liquid displacement porometry have been carried out.

The mercury intrusion is carried out using a mercury porosimeter Quanta-Chrome 33000. A weighed amount of membrane is intruded into the porosimeter chamber, and evacuated to a pressure of 10 μm of Hg for 10 h. After this, mercury is put into the chamber and the pressure is then increased to fill the pores of the membrane with mercury. The pore radius is calculated using the Washburn equation,

$$r = \frac{2\gamma \cos \vartheta}{p_r}$$

where p_r is the pressure at which pores of radius r are intruded; γ is the surface tension (Pa·m) and ϑ is the contact angle (rad). The values of $\vartheta = 126.3°$ and $\gamma = 0.474$ Pa·m have been used.

By monitoring the volume change of mercury and the corresponding pressure, the pore-size distribution of the membrane can be calculated by a computer program (Lowell and Shields, 1987). Figure 1 shows the results obtained for the Millipore membrane, $dV/d \ln p_r$ indicating how the introduced Hg volume changes when the pressure varies.

Some inconveniences that we detected when using the Hg porosimeter technique are described below:

(a) Difficulties in separating the holder of the membrane in the case of Gelman membranes makes the sampling amount of the analyzed membrane small and therefore the results obtained by this technique and for these membranes have not been considered valid.

(b) High pressures used in the mercury intrusion measurement can cause membrane compaction as well as the formation of microfractures with a consequent alteration of pore shape and size.

(c) Mercury cannot differentiate between available pores and nonavailable pores for flow, since it intrudes from all directions. This is because mercury not only intrudes through

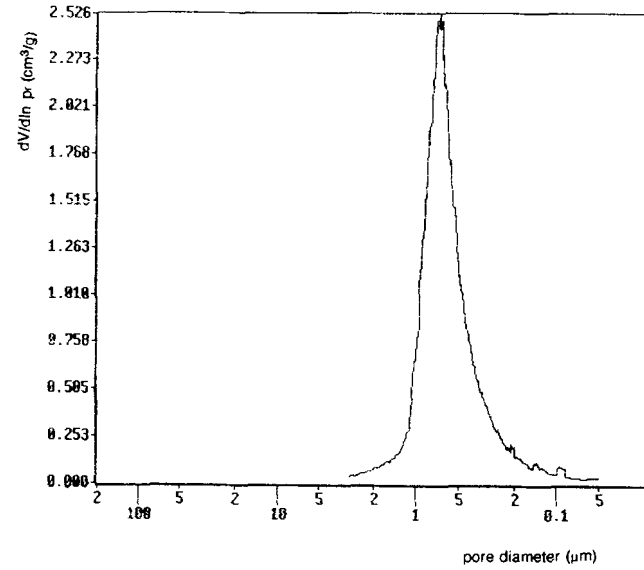

Figure 1. Pore-size distributions of Millipore membrane from mercury porosimetry.

pores that are connected from one side of a membrane to the other, but also through pores that are blocked. However, when dealing with filtration, characterization of the available pores is thought to be very important.

These inconveniences are avoided by using the liquid displacement method. This method does not need any special skills; it is quick and easy and the test results are clearly defined.

A Coulter Porometer II Manufactured by Coulter Electronics Ltd. has been used. This apparatus uses a liquid displacement technique. The sample is first thoroughly wetted with a liquid (Coulter Porofilm) of low surface tension ($\gamma = 16 \times 10^{-3}$ Pa·m), low vapor pressure (3 mm Hg at 298 K), and low reactivity, which is assumed to fill all the pores given that it has a zero contact angle with virtually all materials. The wetted sample is subjected to increasing pressure applied by a compressed clean and dry air source at 313 K. As the pressure of air increases, it will reach a point where it can overcome the surface tension of the liquid in the largest pores and will push the liquid out. According to the Washburn equation, further increasing the pressure allows for the air to flow through smaller pores.

When different pores of diverse sizes are opened, the volume flow of air increases accordingly until all the pores are emptied. By monitoring the applied pressure and the flow of gas through the sample when liquid is being expelled, a wet run is obtained. If the sample is then tested dry (without liquid in its pores), a dry run follows. Thus, the volume flow for the wet run and for the dried one vs. the applied pressure allows us to evaluate several statistical parameters (Venkataraman et al., 1988), among them the differential pore number frequency distribution. The results obtained for the different membranes are given in Figures 2–4 and indicate that these membranes have a narrow pore-size distribution. On the other hand, the comparison of Figures 1 and 4 indicate that the Hg porosimetry gives good results in the case of the Millipore membrane.

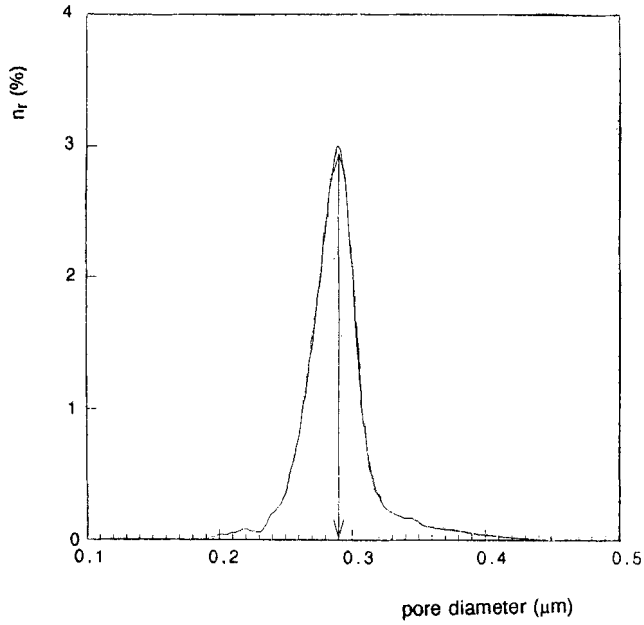

Figure 2. Pore-size distribution of TF 200 membrane from the Coulter porometer.

n_r indicates the relative number of pores with porous radium r.

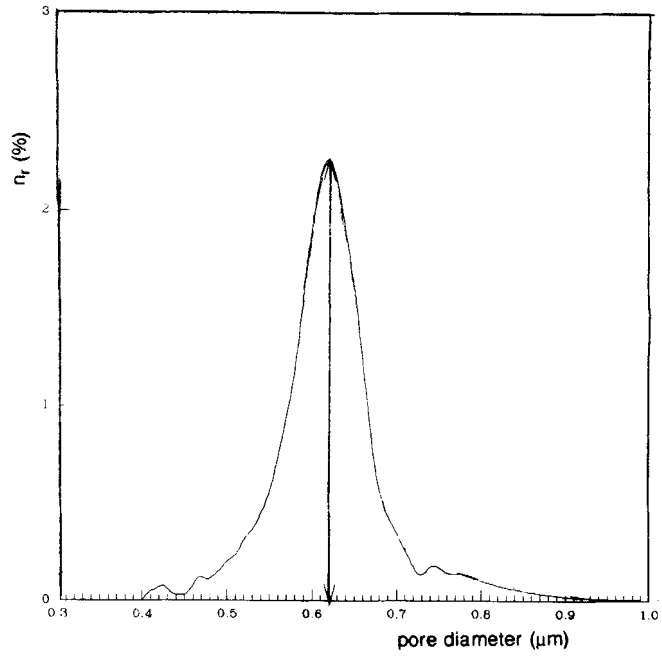

Figure 4. Pore-size distribution of Millipore membrane from the Coulter porometer.

n_r indicates the relative number of pores with porous radium r.

Experimental Setup

The membrane cell is a tangential filtration cell manufactured by Millipore Corporation as Minitan-S (Figure 5). In this membrane cell a flat sheet membrane separates the dis-

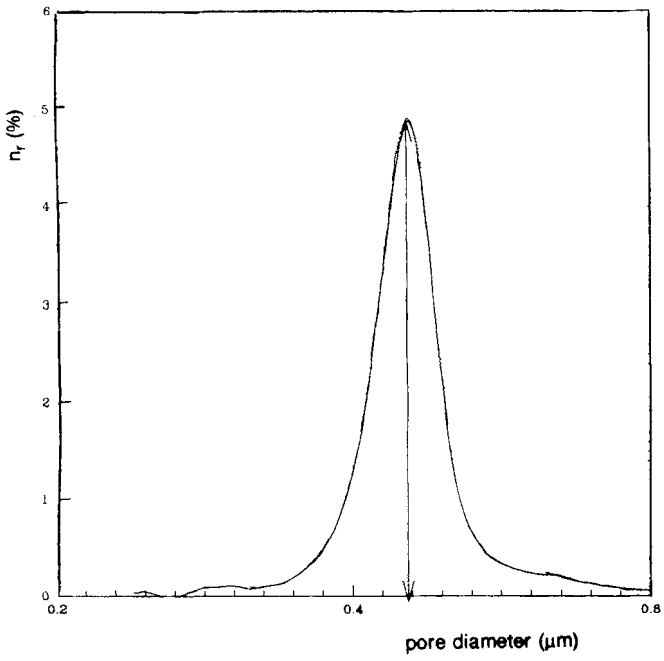

Figure 3. Pore-size distribution of TF 450 membrane from the Coulter porometer.

n_r indicates the relative number of pores with porous radium r.

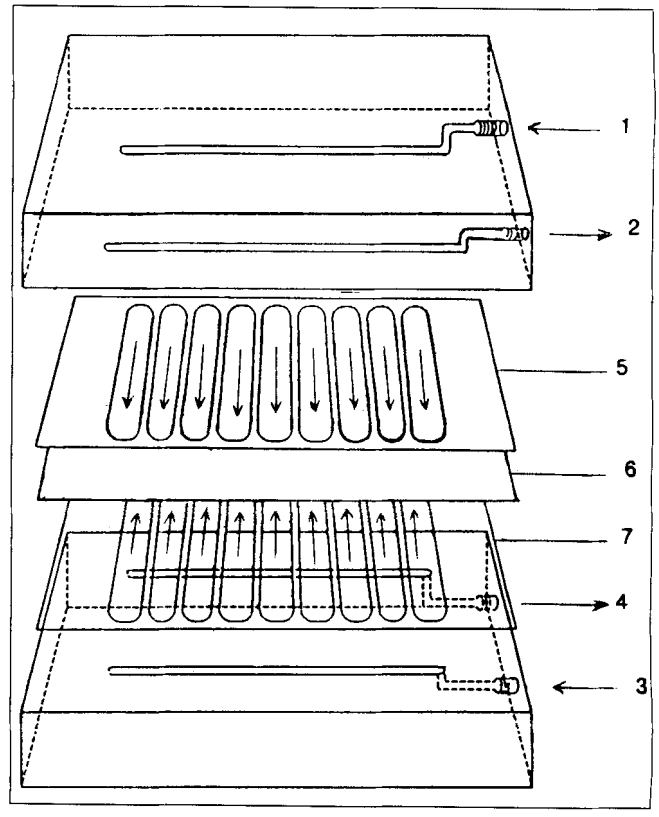

Figure 5. Membrane holder.

Entrance (1) and exit (2) of cold water; entrance (3) and exit (4) of hot water; silicone separators (5) and (7); and membrane (6).

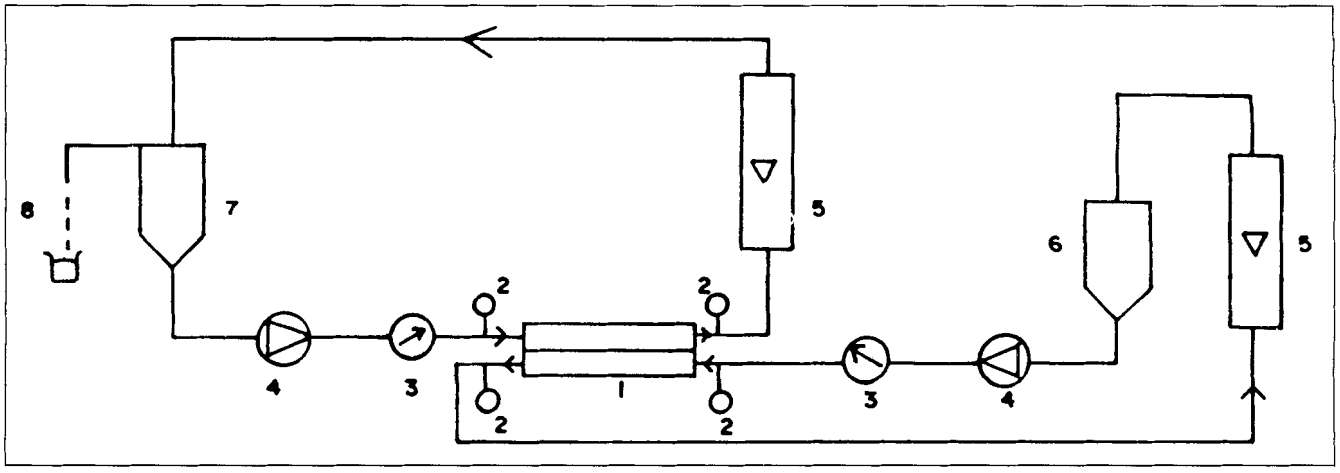

Figure 6. Experimental device.

Membrane cell (1); thermocouple (2); pressure transducer (3); pump (4); flowmeter (5); hot tank (6); cold tank (7); and distillate water (8).

tilland and distillate liquid phases. Both hot (distilland) and cold (distillate) liquid phases are formed by nine prismatic channels (provided by each silicon sheet) of approximately $0.45 \times 7.0 \times 55.0$ mm giving an effective membrane area of 34.65×10^{-4} m^2. The cold and hold liquids are preheated in each corresponding thermostatic bath and are then pumped across the membrane in countercurrent directions (Figure 6).

Flow rate, temperatures, and pressures are monitored as appropriate. The temperatures of the water were measured at the entrance ($T_{b1\text{-in}}$, $T_{b2\text{-in}}$) and exit ($T_{b1\text{-out}}$, $T_{b2\text{-out}}$) of the membrane cell (Figure 7). Average values of the temperature T_{b1}, T_{b2}, T_b (K) and of the temperature difference ΔT_b (K) between the bulk phases at both sides of the membrane were calculated as

$$T_{b1} = \frac{T_{b1\text{-in}} + T_{b1\text{-out}}}{2}$$

$$T_{b2} = \frac{T_{b2\text{-in}} + T_{b2\text{-out}}}{2}$$

$$T_b = \frac{T_{b1} + T_{b2}}{2}$$

$$\Delta T_b = T_{b1} - T_{b2}$$

As mentioned in the Introduction, due to the existence of temperature gradients in the liquid phases adjacent to the membrane, this ΔT_b is higher than the actual temperature difference between both sides of the membrane. The following equation indicates their difference:

$$\Delta T_m = T_{m1} - T_{m2}$$

where T_{m1} (K) and T_{m2} are the average temperatures of the hot and cold membrane sides, respectively.

The distillate flux is measured by timing and weighing the water which overflows out of the capillary attached to the top of the cold reservoir.

In the present work a series of experiments have been performed. In each experiment a temperature difference was maintained between the thermostatic baths, and the corresponding mass flux through the membrane was measured for different flow rates on both sides of the membrane. Different experiments were carried out for different temperatures with each membrane.

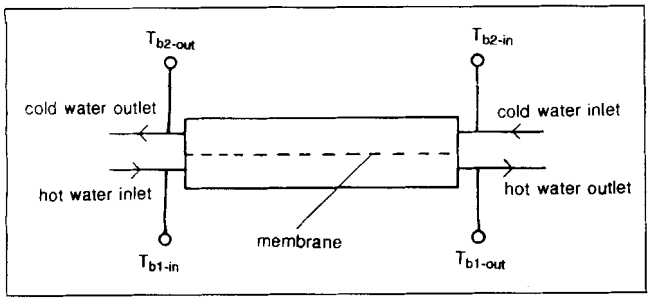

Figure 7. Fundamental process of membrane cell.

Theory

In membrane distillation, coupling between heat and mass transfer arises. The transmembrane temperature difference may not only result in heat transfer, but can also lead to mass transfer. In this case a concentration gradient is set up as a result of the nonuniformity of the temperature T, and the water flux is given according to the theory of Non-Equilibrium Thermodynamics (Katchalsky and Curran, 1967) as

$$J = \frac{\epsilon}{\chi}\left[D\nabla c + L\frac{\nabla T}{T}\right] \tag{1}$$

where ϵ is the membrane porosity, χ the tortuosity factor, D is the diffusion coefficient of water vapor at the average temperature in the membrane (m^2·s^{-1}), c is the water vapor concentration (kg·m^{-3}) (while for low pressures it may change for the expression pM/RT), and L is the coupling coefficient (kg·m^{-1}·s^{-1}). Therefore, the total flow of water vapor is made up of two terms: the diffusion flow proportional to the con-

centration gradient and a thermal diffusion flow dependent on the transmembrane temperature gradient. However as indicated by Katchalsky and Curran (1967) and measured by Banat and Simandl (1994), the thermal diffusion coefficient is found to be smaller by a factor of 10^2 to 10^3 than the ordinary diffusion coefficient for gases which causes the thermal diffusion contribution toward the mass flux through the membrane to be minimal. In this way and for sufficiently small transmembrane temperature differences, the following linear relation between flux and vapor pressure difference can be obtained

$$J = C(p_1 - p_2) \tag{2}$$

This relation is commonly accepted in studies of membrane distillation (Schneider et al., 1988; Schofield et al., 1987; Mengual et al., 1993) showing that the vapor pressure difference through the membrane $(p_1 - p_2)$ determines the J flow rate. In Eq. 2, C is a variable in general, depending on pore geometry, gas pressure, temperature, and gaseous species. The determination of C under any given condition requires an understanding of the various permeation mechanisms.

In our case especially, and in order to be able to explain the transport through the membrane, the following diffusion mechanisms must be taken into account:

(a) Due to the existence of noncondensable gases (air) in the pores of the membrane which act as a stagnant film, the molecular diffusion model must be applied, and so (Bird et al., 1960)

$$J_D = \frac{1}{Y_{\ln}} \frac{D\epsilon}{\chi\delta} \frac{M}{RT}(p_1 - p_2) \tag{3}$$

where D is the water vapor diffusion coefficient, M the water molecular weight ($kg \cdot mol^{-1}$), δ the membrane thickness (m), $Y_{\ln}$ the logarithm of the mole fraction of air (log mean), and R the gas constant ($J \cdot mol^{-1} \cdot K^{-1}$).

(b) However as the pore sizes and the mean free molecular paths in the membrane distillation process are of the same order of magnitude, the Knudsen diffusion must be taken into account. Knudsen diffusion is a gas transport mechanism whereby gas molecules under a pressure gradient pass through a porous structure by a series of molecule/wall collisions. For gas permeation through a microporous membrane, the Knudsen diffusion equation may be written as (Present, 1958)

$$J_k = \frac{2}{3} \frac{r\epsilon}{\chi\delta} \sqrt{\frac{8M}{\pi RT}}(p_1 - p_2) \tag{4}$$

The two models mentioned suggest Eq. 2 for the mass transfer, where C can be considered a combined transmembrane mass-transfer coefficient ($kg \cdot m^{-2} \cdot s^{-1} \cdot Pa^{-1}$), accounting for the mass-transfer resistances of both molecular and Knudsen diffusions. Inspection of both models suggests that C will be slightly temperature-dependent, decreasing $< 3\%$ with a 10°C increase in mean temperature.

As vapor pressures within the membrane are not directly measurable, it is convenient to express Eq. 2 in terms of temperatures

$$J = C\left[\frac{dp}{dT}\right]_{T_m}(T_{m_1} - T_{m_2}) \tag{5}$$

Equation 5 is a good approximation for values of $T_{m1} - T_{m2} < 10°C$. In addition, dp/dT can be evaluated from the Clausius-Clapeyron equation at the T_m average membrane temperature. Since, as opposed to the temperatures T_{b1} and T_{b2}, the temperatures T_{m1} and T_{m2} are difficult to measure, T_{b1} and T_{b2} are, as a rule, inserted in the above equation. In order to do this, we must use the heat-transfer coefficients (h_1, h_2) $(W \cdot m^{-2} \cdot K^{-1})$ in the liquid films near the membrane, the latent heat transfer (λ) accompanying the vapor flux $(J \cdot kg^{-1})$, and the heat transfer by conduction (k_m) $(W \cdot m^{-1} \cdot K^{-1})$ across the membrane. In this way, for the stationary transmembrane thermal flux across the membrane system we can write

$$h_1(T_{b1} - T_{m1}) = \frac{k_m}{\delta}(T_{m1} - T_{m2}) + J\lambda = h_2(T_{m2} - T_{b2}) \tag{6}$$

Equations 5 and 6 show that the process is characterized by a simultaneous mass and heat transfer in the membrane and in the external liquid phases. In fact, as indicated by Eq. 5, the driving force for a transmembrane mass transfer is related to the temperature difference between the evaporation and condensation surfaces $T_{m1} - T_{m2}$, which in turn, as indicated by Eq. 6, depends on the heat-transfer rate in the liquid phases. Thus, the overall process rate appears to be controlled by two simultaneous processes: a heat transfer in the liquid phases and a mass transfer across the membrane. We will discuss the relative role played by both actions by introducing the polarization coefficient τ

$$\tau = \frac{T_{m1} - T_{m2}}{T_{b1} - T_{b2}}$$

As an example, in the case of a very fast heat transfer in the liquid phases, the T_{m1} temperature approaches the bulk temperature T_{b1}, and T_{m2} to T_{b2}, resulting that $\tau \to 1$; in this case the process rate is completely controlled by the transmembrane mass-transfer resistance.

On the other hand, for a low heat-transfer value and a large C value, the T_{m1} approaches to T_{m2} and $\tau \to 0$; in this case the process rate is completely controlled by the heat-transfer resistance in the liquid phases.

In order to calculate τ, we can deduce from Eqs. 5 and 6

$$T_{m1} - T_{m2} = \frac{1}{1 + \frac{H}{h_1} + \frac{H}{h_2}}(T_{b1} - T_{b2}) = \tau(T_{b1} - T_{b2}) \tag{7}$$

where

$$H = C\lambda\frac{dp}{dT} + \frac{k_m}{\delta} \tag{8}$$

and

$$\tau = \frac{1}{1+\frac{H}{h_1}+\frac{H}{h_2}} = \frac{1}{1+\frac{H}{h}} \tag{9}$$

with $h = 1/(1/h_1 + 1/h_2)$ being the overall film heat-transfer coefficient in the liquid boundary layers of the membrane.

On the other hand, from Eqs. 5 and 7

$$\frac{T_{b1} - T_{b2}}{J\lambda} = \frac{1+\frac{k_m}{\delta h}}{C\lambda\frac{dp}{dT}} + \frac{1}{h} \tag{10}$$

which allows us to calculate for C and h, and therefore for τ.

Results and Discussion

As previously mentioned, experiments were carried out for fixed temperatures in the membrane module. In all the experiments $\Delta T_b = 10°C$, while the average temperatures T_{b1} varied from 20 to 50°C at steps of about 7°C, and T_{b2} from 10° to 40°C, also at steps of about 7°C.

In each experiment the liquid recirculation rate v ($m^3 \cdot s^{-1}$) was the same (except for small fluctuations, always under 5%) on both sides of the membrane. This rate varied in the different experiments from 5.0 ± 0.2 cm^3/s (which is a shear rate of about 17.6 cm/s over the membrane) to 15.0 ± 0.6 cm^3/s (about 52.9 cm/s over the membrane). The transmembrane pressure gradient was minimum for all the experiments while the absolute pressure in the membrane varied from 10^5 Pa for the lower recirculation rate and up to 1.3×10^5 Pa for the higher recirculation rate.

The flux results shown in Figures 8–10 show how the distillate flux increases monotonically with the recirculation rate. This increase corresponds to a decrease of the heat resistance in the liquid boundary layers of the membrane. Also, the distillate flux increases when the absolute temperature level in the membrane increases, corresponding to an increase of dp/dT with temperature.

On the other hand, as these results show, an important role is played by the membrane thickness; indeed two com-

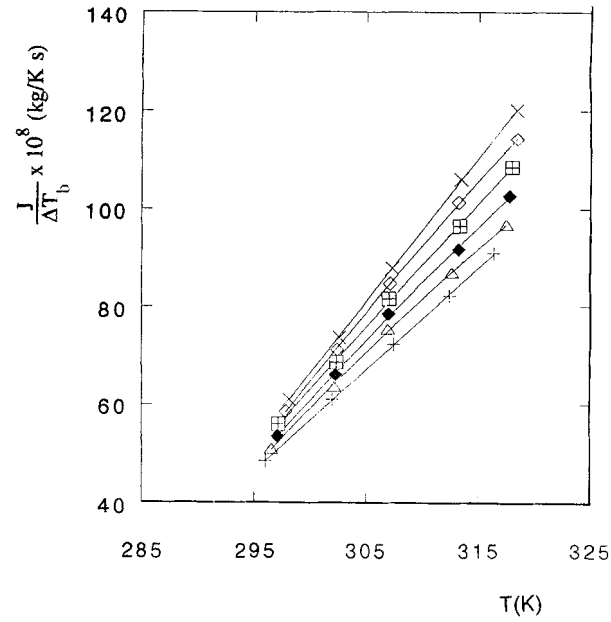

Figure 9. Water flux through TF 450 membrane vs. average temperature.

Recirculation rates: +, 5 $cm^3 \cdot s^{-1}$; Δ, 7 $cm^3 \cdot s^{-1}$; ♦, 9 $cm^3 \cdot s^{-1}$; ⊞, 11 $cm^3 \cdot s^{-1}$; ◇, 13 $cm^3 \cdot s^{-1}$; x, 15 $cm^3 \cdot s^{-1}$.

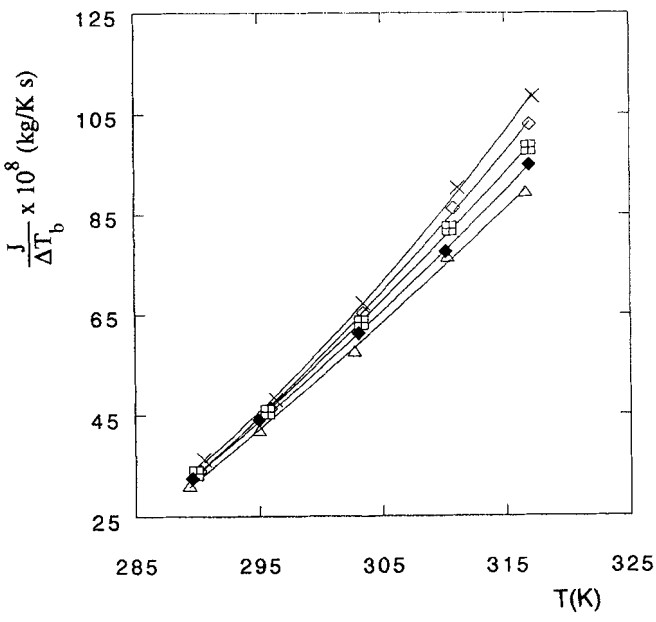

Figure 8. Water flux through TF 200 membrane vs. average temperature.

Recirculation rates: Δ, 7 $cm^3 \cdot s^{-1}$; ♦, 9 $cm^3 \cdot s^{-1}$; ⊞, 11 $cm^3 \cdot s^{-1}$; ◇, 13 $cm^3 \cdot s^{-1}$; x, 15 $cm^3 \cdot s^{-1}$.

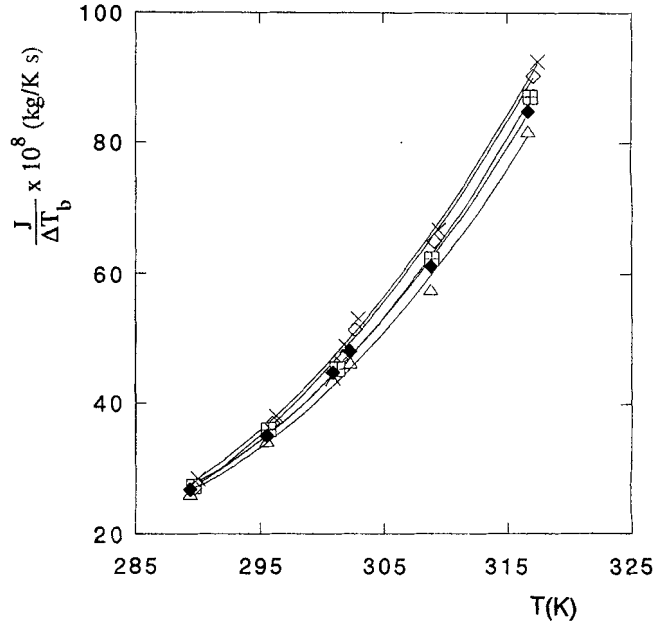

Figure 10. Water flux through Millipore membrane vs. average temperature.

Recirculation rates: Δ, 7 $cm^3 \cdot s^{-1}$; ♦, 9 $cm^3 \cdot s^{-1}$; ⊞, 11 $cm^3 \cdot s^{-1}$; ◇, 13 $cm^3 \cdot s^{-1}$; x, 15 $cm^3 \cdot s^{-1}$.

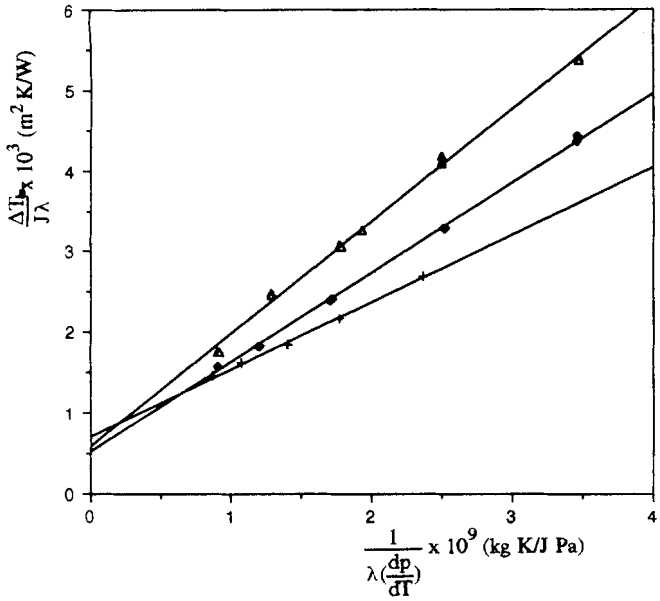

Figure 11. $\Delta T_b/J\lambda$ vs. $1/\lambda(dP/dT)$ corresponding to the flux results.

TF 200 (♦), TF 450 (+), and Millipore (Δ) membranes when the recirculation rate was 7 $cm^3 \cdot s^{-1}$.

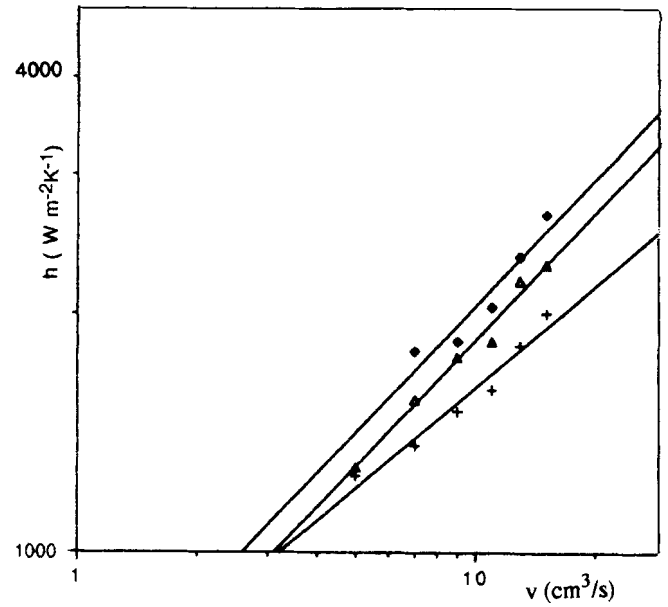

Figure 12. Overall film heat-transfer coefficient ($W \cdot m^{-2} \cdot K^{-1}$) vs. recirculation rate ($cm^3 \cdot s^{-1}$).

TF 200 (♦), TF 450 (+), and Millipore (Δ) membranes.

peting effects are present: an increase in the thickness leads to a greater diffusion resistance, while the effective temperature difference ΔT_m is also increased. Taking into account Eq. 5, we conclude that the first effect overcomes the second as we see that the mass flux for the Millipore membrane is less than that of the TF450 membrane. Therefore the permeate flux decreases when the membrane thickness increases.

Plots of Eq. 10 for the experimental water flux corresponding to the same recirculation rate and different average temperatures have been carried out in order to evaluate h and C, resulting in plots having a correlation coefficient > 0.99. In this equation, dp/dT is evaluated for the T_m (K) average temperature. In order to minimize errors in all the experiments the overall temperature difference is only 10°C. In the same way, for the different experiments, the $T_{b1-in} - T_{b1\text{-out}}$ and $T_{b2\text{-out}} - T_{b2\text{-in}}$ differences were little (between 0.2 and 1.5°C, depending on the different recirculation rates). Representative plots of Eq. 10 are shown in Figure 11.

The h values obtained from the intercept of plots of Eq. 10 are shown in Figure 12 as a function of the recirculation rate; the data are well fitted by the power law relationship, $h = Av^{\alpha}$ with R correlation coefficients, and α values of

TF200:	$\alpha = 0.54$	$R = 0.95$
TF450:	$\alpha = 0.54$	$R = 0.98$
Millipore:	$\alpha = 0.43$	$R = 0.98$

These α values are in good keeping with the value of 0.5 obtained by different authors (Holman, 1989; Porter, 1972) for a laminar regime on a flat.

The differences in the absolute values of h for the different membranes are attributed to the differences that can be found in the height of the water circulation channels on both sides of the membrane, which has only approximately been estimated at 0.45 mm.

In order to evaluate the C coefficients from the slope of plots of Eq. 10, the thermal conductivity of the porous membranes k_m was calculated as

$$k_m = \epsilon k_g + (1 - \epsilon) k_s$$

where k_g and k_s are the thermal conductivities of the gas phase (0.027 $W \cdot m^{-1} \cdot K^{-1}$) and of the solid phase (0.22 $W \cdot m^{-1} \cdot K^{-1}$ for the PTFE and 0.126 $W \cdot m^{-1} \cdot K^{-1}$ for the PVDF) (Perry, 1963; Speraty, 1989). In this way, the following values of C are obtained

$$C \text{ (TF 200)} = (14.5 \pm 0.8) \times 10^{-7} \text{ kg} \cdot \text{m}^{-2} \cdot \text{s}^{-1} \cdot \text{Pa}^{-1}$$

$$C \text{ (TF 450)} = (21.5 \pm 1.0) \times 10^{-7} \text{ kg} \cdot \text{m}^{-2} \cdot \text{s}^{-1} \cdot \text{Pa}^{-1}$$

$$C \text{ (Millipore)} = (9.1 \pm 0.5) \times 10^{-7} \text{ kg} \cdot \text{m}^{-2} \cdot \text{s}^{-1} \cdot \text{Pa}^{-1}$$

These results are independent of the recirculation rate in the system. The TF 200 and TF 450 membranes are two membranes with similar structural characteristics; so, given that the obtained values of C are in the same relation as the average diameters of the pore obtained for them (0.3 and 0.45 μm, respectively), the transport mechanism of the water vapor in these membranes would be predominantly of a Knudsen type. For the Millipore 450 membrane, which only has a slightly superior pore size (although having a double thickness compared to TF membranes), it may also be expected that this type of transport mechanism would be a predominant one. Therefore, although it is possible that the air within the pores could be removed by diffusion in the bulk liquid phases, this would not affect the results obtained.

Finally, the experimental C and h values allow us to quantify the τ temperature polarization coefficient. Figures 13–15 show the results obtained for the three membranes, calcu-

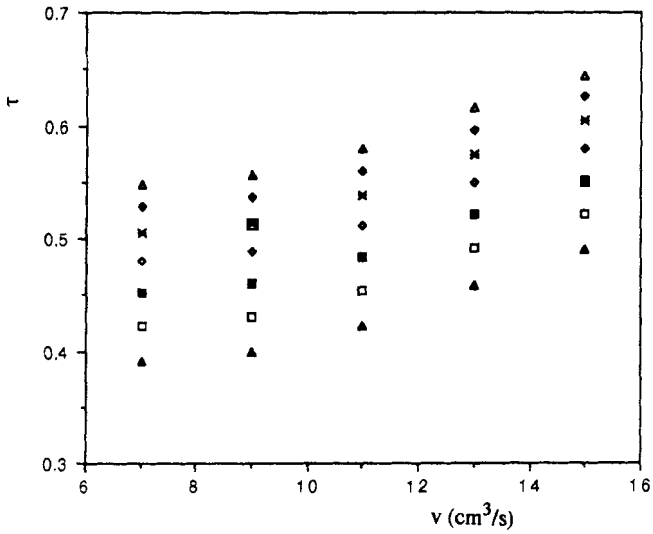

Figure 13. Temperature polarization coefficient vs. recirculation rate of the TF 200 membrane.

Average temperatures: Δ, 15°C; ♦, 20°C; *, 25°C; ◇, 30°C; ■, 35°C; □, 40°C; ▲, 45°C.

lated according to Eqs. 8 and 9. These results have provided us with useful information to draw the following important conclusions.

Conclusions

(1) A TF 450 membrane has a high polarization temperature coefficient ($\tau < 0.5$) for the temperatures and recirculation rates studied. For this membrane, the mass flux is heat-transfer controlled. On the other hand, the Millipore membrane has a low polarization temperature coefficient ($\tau > 0.5$) indicating that the mass flux is predominantly controlled by the mass-transfer resistance through the membrane. An intermediate behavior is present in the TF 200 membrane ($\tau \sim 0.5$).

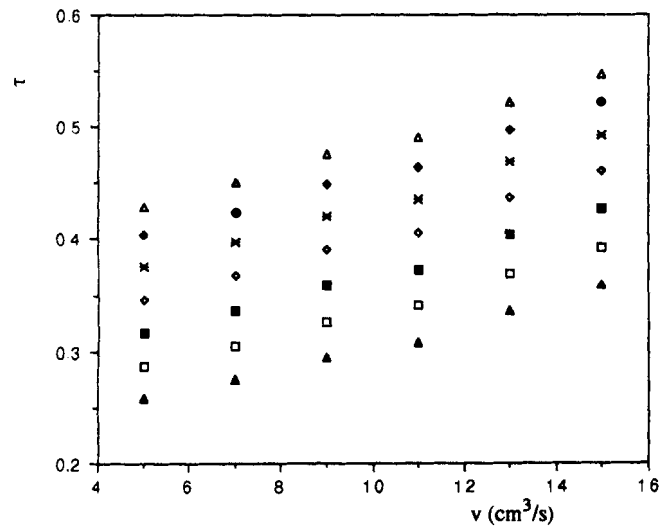

Figure 14. Temperature polarization coefficient vs. recirculation rate of the TF 450 membrane.

Symbols as for Figure 13.

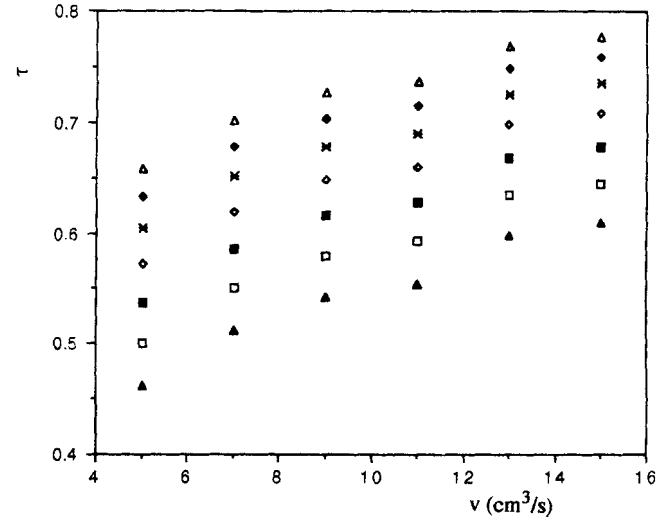

Figure 15. Temperature polarization coefficient vs. recirculation rate of the Millipore membrane.

Symbols as for Figure 13.

(2) For all the membranes, the larger mass fluxes obtained as the temperature increases, involve more important heat fluxes through the liquid phases, so that the resistance offered by a heat transfer in the liquid phases increases with respect to the resistance to a transmembrane mass transport. In fact, Figures 13–15 show how τ decreases with temperature.

(3) We wish to point out, as shown in Figures 8–10, that the mass flux is affected more by the recirculation rate in a TF-450 membrane than in a Millipore membrane in relation to the fact that in the first case the flux is heat-transfer controlled in a larger measurement than for the Millipore membrane. In other words, the changes in the feed fluid dynamics affect the process rate, essentially through the changes induced in the temperature polarization.

(4) Finally, it is necessary to conclude that any attempt to explain any membrane distillation results must take into account the significant influence of temperature polarization. This is clear when the results obtained from the TF 450 membrane are compared with those of the Millipore membranes. The first has a double C membrane coefficient when compared to the second, but the mass flux in the first is only slightly superior to that of the second. In the first the polarization temperature is more important than in the second.

Notation

∇c = concentration gradient, $kg \cdot m^{-4}$
H = membrane heat-transfer coefficient, $W \cdot m^{-2} \cdot K^{-1}$
J = mass flux, $kg \cdot m^{-2} \cdot s^{-1}$
k_g = thermal conductivity of the air, $W \cdot m^{-1} \cdot K^{-1}$
k_s = thermal conductivity of the solid phase of the membrane, $W \cdot m^{-1} \cdot K^{-1}$
p = pressure of water vapor, Pa
p_r = pressure at which pores of radius r are intruded of Hg, $N \cdot m^{-2}$
r = membrane pore radius, m
V = volume of intruded Hg

Subscripts

D = molecular diffusion model
K = Knudsen diffusion model

Literature Cited

Anderson, S., N. Kjellander, and B. Rodesjö, "Design and Field Tests of a New Membrane Distillation Desalination Process," *Desalination*, **56**, 345 (1985).

Banat, F. A., and J. Simandl, "Theoretical and Experimental Study in Membrane Distillation," *Desalination*, **95**, 39 (1994).

Bellucci, F., "Temperature Polarization Effects in Thermoosmosis," *J. Membr. Sci.*, **9**, 285 (1981).

Bird, R. B., W. E. Stewart, and E. N. Lightfoot, *Transport Phenomena*, Wiley, New York (1960).

Calabro, V., E. Drioli, and F. Matera, "Membrane Distillation in the Textile Wastewater Treatment," *Desalination*, **83**, 209 (1991).

Calabro, V., G. Pantano, M. Kang, R. Molinari, and E. Drioli, "Experimental Study on Integrated Membrane Processes in the Treatment of Solutions Simulating Textile Effluents. Energy and Exergy Analysis," *Desalination*, **78**, 257 (1990).

Drioli, E., and Y. Wu, "Membrane Distillation: An Experimental Study," *Desalination*, **53**, 339 (1985).

Enoch, G. D., W. F. van den Broeke, and W. Spiering, "Removal of Heavy Metals and Suspended Solids from Wastewater from Wet Lime (Stone)-Gypsum Flue Gas Desulphurization Plants by Means of Hydrophobic and Hydrophilic Crossflow Microfiltration Membranes," *J. of Memb. Sci.*, **87**, 191 (1994).

Gostoli, C., and G. Sarti, "Separation of Liquid Mixtures by Membrane Distillation," *J. Memb. Sci.*, **41**, 211 (1989).

Hoffmann, E., D. M. Pfenning, E. Philipsen, P. Schwahn, M. Sieber, R. Wehn, and D. Woermann, "Evaporation of Alcohol/Water Mixtures Through Hydrophobic Porous Membranes," *J. Memb. Sci.*, **34**, 199 (1987).

Holman, J. P., *Heat Transfer*, McGraw-Hill, New York, p. 231 (1989).

Katchalsky, A., and P. F. Curran, *Non-Equilibrium Thermodynamics in Biophysics*, Harvard Univ. Press, Cambridge, MA (1967).

Lowell, S., and J. E. Shields, *Powder Surface Area and Porosity*, Powder Technol. Ser., B. Scarlett, ed., Wiley, New York (1987).

Mengual, J. I., J. M. Ortíz de Zárate, L. Peña, and A. Velázquez, "Osmotic Distillation Through Porous Hydrophobic Membranes," *J. Memb. Sci.*, **82**, 129 (1993).

Nakao, S., F. Saitoh, T. Asakura, K. Toda, and S. Kimura, "Continuous Ethanol Extraction by Pervaporation from a Membrane Bioreactor," *J. Memb. Sci.*, **30**, 273 (1987).

Ohta, K., K. Kikuchi, I. Hayano, T. Okabe, T. Goto, S. Kimura, and H. Ohya, "Experiments on Sea Water Desalination by Membrane Distillation," *Desalination*, **78**, 177 (1990).

Perry, J. H., *Chemical Engineers Handbook*, 4th ed., McGraw-Hill, New York (1963).

Porter, M. C., "Concentration Polarization with Membrane Ultrafiltration," *Ind. Eng. Chem. Prod. Res. Dev.*, **11**(3), 234 (1973).

Present, R. D., *The Kinetic Theory of Gases*, McGraw-Hill, New York (1958).

Schneider, K., W. Hölz, R. Wollbeck, and S. Ripperger, "Membranes and Modules for Transmembrane Distillation," *J. Memb. Sci.*, **39**, 25 (1988).

Schofield, R. W., A. G. Fane, and C. J. D. Fell, "Heat and Mass Transfer in Membrane Distillation," *J. Memb. Sci.*, **33**, 299 (1987).

Sheng, J., R. A. Johnson, and M. S. Léfèbvre, "Mass and Heat Transfer Mechanism in the Osmotic Distillation Process," *Desalination*, **80**, 113 (1991).

Speraty, C. A., "Physical Constants of Fluoropolymers," *Polymer Handbook*, 3rd ed., Wiley, New York (1989).

Venkataraman, K., W. T. Choate, E. R. Torre, R. D. Husung, and H. R. Batchu, "Characterization Studies of Ceramic Membranes. A Novel Technique Using a Coulter Porometer," *J. Memb. Sci.*, **39**, 259 (1988).

Vink, H., and S. A. A. Chisthi, "Thermal Osmosis in Liquids," *J. Memb. Sci.*, **1**, 149 (1976).

Manuscript received July 28, 1995, and revision received Oct. 26, 1995.